Acta Crystallographica Section F
Structural Biology and Crystallization Communications
ISSN 1744-3091

Structure of the adenylation domain of NAD$^+$-dependent DNA ligase from *Staphylococcus aureus*

Seungil Han,* Jeanne S. Chang and Matt Griffor

Pfizer Inc., Pfizer Global Research and Development, Eastern Point Road, Groton, Connecticut 06340, USA

Correspondence e-mail: seungil.han@pfizer.com

Received 7 July 2009
Accepted 11 September 2009

PDB References: SauLigA, 3jsl, r3jslsf; 3jsn, r3jsnsf.

DNA ligase catalyzes phosphodiester-bond formation between immediately adjacent 5′-phosphate and 3′-hydroxyl groups in double-stranded DNA and plays a central role in many cellular and biochemical processes, including DNA replication, repair and recombination. Bacterial NAD$^+$-dependent DNA ligases have been extensively characterized as potential antibacterial targets because of their essentiality and their structural distinction from human ATP-dependent DNA ligases. The high-resolution structure of the adenylation domain of *Staphylococcus aureus* NAD$^+$-dependent DNA ligase establishes the conserved domain architecture with other bacterial adenylation domains. Two apo crystal structures revealed that the active site possesses the preformed NAD$^+$-binding pocket and the 'C2 tunnel' lined with hydrophobic residues: Leu80, Phe224, Leu287, Phe295 and Trp302. The C2 tunnel is unique to bacterial DNA ligases and the Leu80 side chain at the mouth of the tunnel points inside the tunnel and forms a narrow funnel in the *S. aureus* DNA ligase structure. Taken together with other DNA ligase structures, the *S. aureus* DNA ligase structure provides a basis for a more integrated understanding of substrate recognition and catalysis and will be also be of help in the development of small-molecule inhibitors.

1. Introduction

Bacterial DNA ligase (EC 6.5.1.2) represents an attractive antibacterial target owing to its essentiality and its conservation throughout eubacteria (Wilkinson *et al.*, 2001). DNA ligase catalyzes phosphodiester-bond formation between immediately adjacent 5′-phosphate and 3′-hydroxyl groups in double-stranded DNA and plays a central role in many cellular and biochemical processes, including DNA replication, repair and recombination (Kornberg & Baker, 1992; Lindahl & Barnes, 1992; Tomkinson *et al.*, 2006). Depending on the cofactor requirement, DNA ligases can be divided into two classes. Eukaryotic cells possess a number of different DNA ligases that use ATP, whereas all eubacterial enzymes use NAD$^+$ to produce AMP and NMN in the course of DNA ligation (Timson *et al.*, 2000; Wilkinson *et al.*, 2001).

Staphylococcus aureus is a Gram-positive bacterial pathogen that is one of the most common causes of hospital- and community-acquired infections, including skin and soft-tissue infections, pneumonia, osteomyelitis and systemic infections. An increasing incidence of methicillin resistance and more recently vancomycin resistance in *S. aureus* is now posing serious health issues (Lowy, 1998; Furuya & Lowy, 2006). Since there are few antibiotics on the market to combat *S. aureus* resistance, there is a pressing need to identify new targets and develop novel antibacterial agents.

Because of their essentiality and their structural distinction from human ATP-dependent DNA ligases, bacterial NAD$^+$-dependent DNA ligases have been extensively characterized as potential antibacterial targets. The crystal structure of the full-length *Thermus filiformis* NAD$^+$-dependent DNA ligase (TfiLigA) revealed a monomeric modular architecture with a unique circular arrangement of four distinct domains: an adenylation domain, a nucleotide-binding (OB-fold) core linked to a zinc-finger domain, a helix–hairpin–helix (HhH) domain and a BRCA1 C-terminal repeat (BRCT) domain

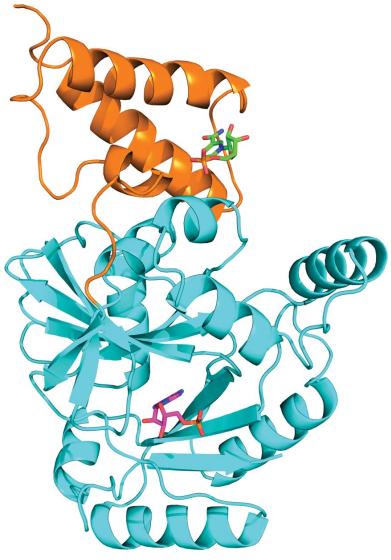

(Lee *et al.*, 2000). The crystal structure of *Escherichia coli* NAD$^+$-dependent DNA ligase (EcoLigA) complexed with a nicked DNA-adenylate intermediate provided insights into nick recognition and the nucleotidyl transfer reaction (Nandakumar *et al.*, 2007). Several structures of the adenylation domains from *Bacillus stearothermophilus* LigA (BstLigA), *Enterococcus faecalis* LigA (EfaLigA) and *Mycobacterium tuberculosis* LigA (MtuLigA) have provided details of the cofactor-binding site and the adenylation step of the reaction (Singleton *et al.*, 1999; Gajiwala & Pinko, 2004; Srivastava, Tripathi *et al.*, 2005).

S. aureus NAD$^+$-dependent DNA ligase (SauLigA) is a 667-residue protein with a calculated mass of 75 080 Da; it has 45–60% amino-acid identity to other bacterial DNA ligases and has a similar modular architecture consisting of four distinct domains (Kaczmarek *et al.*, 2001). The N-terminal adenylation domain of SauLigA (molecular weight 35 851 Da) contains the cofactor-binding site and the active-site lysine. To elucidate the catalytic mechanism of eubacterial DNA ligase and its substrate specificity, we determined the structure of the adenylation domain of *S. aureus* DNA ligase in order to examine an NAD$^+$-dependent DNA ligase from a clinically relevant Gram-positive pathogen. Our structural analysis provides insights into the mechanism of bacterial DNA ligase substrate recognition and the potential for the rational design of selective SauLigA inhibitors.

2. Materials and methods

2.1. Protein cloning, expression and purification

Expression vector pMCG545 was prepared by amplifying the *S. aureus* DNA ligase gene with the forward primer 5′-GGAATTC**CATATG**GCTGATTTATCGTCTCGTGTG-3′ and the reverse primer 5′-CCG**CTCGAG**CTATCAATGGTGATGGTGATGATGTTCCTCAGCTGGAAATTTATAAGC-3′ (restriction sites are shown in bold). The reverse primer incorporates a His_6 tag. After ligation into the vector pET29b(+) at the *Nde*I and *Xho*I sites, the protein expressed from this construct yields *S. aureus* DNA ligase Met1–Glu312 followed by a His_6 tag. The DNA was transformed into BL21 (DE3) cells for expression. 1 ml of an overnight inoculum was used to inoculate 1 l LB containing 50 µg ml^{-1} kanamycin. The culture was grown at 310 K until an OD_{600} of 0.75 was reached and was then induced with IPTG at a final concentration of 0.6 m*M*. The culture was harvested 3 h post-induction. Alternatively, the cultures were induced with a 50 µ*M* final concentration of IPTG with continued shaking at 293 K overnight.

The protein was purified as described for EfaLigA (Gajiwala & Pinko, 2004) with a few modifications. All steps were performed at 277 K. Frozen harvested cell pellets were resuspended in lysis buffer (25 m*M* potassium phosphate pH 8.0 and 250 m*M* NaCl) at a volume of three times their wet weight. One EDTA-free protease-inhibitor cocktail tablet (Roche) and 1 µl Benzonase nuclease (Sigma) were added per 50 ml cell suspension. The cells were lysed using sonication (Branford Sonifier) and the cell debris was removed by centrifugation at 12 000 rev min^{-1} in an SS-34 rotor (Sorvall) for 20 min. The resulting supernatant was filtered and applied onto pre-packed HisTrap FF crude columns (3 × 5 ml; GE Healthcare) that had been equilibrated in lysis buffer plus 20 m*M* imidazole. After washing with 5–10 column volumes (CV) of lysis buffer plus 20 m*M* imidazole, the column was then eluted with a linear gradient of lysis buffer plus 20–300 m*M* imidazole in 3.33 CV. The peak was pooled and dialyzed into a low-salt buffer (25 m*M* Tris pH 8.0 and 20 m*M* NaCl) appropriate for ion-exchange chromatography. The dialyzed protein was loaded onto a HiPrep Q XL 16/10 column (GE Healthcare) that had been equilibrated in low-salt buffer. The column was then washed with 5–10 CV of low-salt buffer and eluted with a linear gradient of low-salt buffer plus 0–1000 m*M* NaCl in 10 CV. The largest peak was pooled and applied directly onto a 20 ml ceramic hydroxyapatite type I column (Bio-Rad) which had been equilibrated with CHTI buffer (25 m*M* Tris pH 8.0 and 200 m*M* NaCl). After washing with 5–10 CV of CHTI buffer, the protein was eluted with a linear gradient of CHTI buffer plus 0–100 m*M* potassium phosphate in 6 CV. The CHTI fractions were then pooled and concentrated to 10 mg ml^{-1} using an Amicon Ultra-15 centrifugal filter device with a 10 kDa molecular-weight cutoff (Millipore). To deadenylate the protein, β-NMN (Sigma) and $MgCl_2$ (Hampton Research) were added to the protein to final concentrations of 10 and 5 m*M*, respectively. The full deadenylation of the protein was tracked by liquid-chromatography electrospray ionization mass spectrometry. After overnight incubation, the protein was desalted into a final buffer of 25 m*M* Tris pH 8.0 and 150 m*M* NaCl using a HiPrep 26/10 column (GE Healthcare). The protein, which was greater than 95% pure as shown by SDS–PAGE, was then concentrated to 40–55 mg ml^{-1} for crystallization experiments.

Table 1
Data-collection and refinement statistics for apo SauLigA.

Values in parentheses are for the highest resolution shell.

	Apo1	Apo2
Data-collection statistics		
Space group	$P1$	$P2_12_12_1$
Resolution range (Å)	50.0–1.8 (1.86–1.8)	30.0–1.9 (1.97–1.9)
Observations		
Overall	112406	107127
Unique	57629	25917
Completeness (%)	95.5 (85.2)	92.6 (74.7)
R_{merge}† (%)	5.4 (22.9)	8.1 (33.8)
$I/\sigma(I)$	15.9 (2.2)	16.5 (3.3)
Refinement statistics		
Resolution range (Å)	30.0–1.8	30.0–1.9
No. of reflections	54693	24543
R factors (%)		
R_{cryst}‡	19.6	19.3
R_{free}§	25.0	23.5
No. of non-H atoms		
Protein	4988	2415
Solvent	471	167
Sulfate	40	
Average temperature factor (Å^2)		
Protein	22.8	31.5
Solvent	30.1	39.5
Sulfate	42.2	
R.m.s.d. from ideal values		
Bond lengths (Å)	0.013	0.022
Bond angles (°)	1.334	1.931
Ramachandran plot (%)		
Most favorable region	92.5	93.3
Outliers	0	0

† $R_{merge} = \sum_{hkl}\sum_i |I_i(hkl) - \langle I(hkl)\rangle| / \sum_{hkl}\sum_i I_i(hkl)$, where $I_i(hkl)$ is the intensity of the ith measurement of reflection hkl and $\langle I(hkl)\rangle$ is the average value over multiple measurements. ‡ $R_{cryst} = \sum_{hkl} ||F_{obs}| - |F_{calc}|| / \sum_{hkl} |F_{obs}|$ for all reflections (no σ cutoff), where F_{obs} and F_{calc} are the observed and calculated structure factors, respectively. § R_{free} was calculated against 5% of the reflections removed at random.

2.2. Crystallization

Apo SauLigA crystals belonging to space group $P1$ (unit-cell parameters $a = 40.15$, $b = 49.19$, $c = 88.0$ Å, $\alpha = 90.1$, $\beta = 103.2$, $\gamma = 90.0°$; two molecules per asymmetric unit) were grown by hanging-drop vapor diffusion from drops containing 2.1–2.5 *M* ammonium sulfate and 0.1 *M* MES or HEPES pH 6.8–7.5. Spherical crystals appeared over the course of several days at 287 K. Subsequently, crystals belonging to the orthorhombic space group $P2_12_12_1$ (unit-cell parameters a = 42.88, b = 79.80, c = 101.68 Å; one molecule per asym-

metric unit) were obtained using a reservoir containing 1.6 *M* DL-malic acid pH 7.0. Thin rod-shaped crystals appeared over the course of several days at 287 K.

2.3. Data collection

The apo SauLigA crystals were transferred to a cryoprotectant solution made up of the reservoir solution with 15% glycerol and were then flash-frozen in a stream of cold nitrogen gas at 100 K. A full data set was collected from one crystal frozen in this manner on an ADSC Quantum 210 CCD detector at the Advanced Photon Source, Argonne National Laboratory. Data were processed using the *HKL*-2000 software suite (Otwinowski & Minor, 1997). Data-collection statistics are summarized in Table 1.

2.4. Structure determination

The structure of the triclinic SauLigA crystal was solved by molecular-replacement methods with the *CCP*4 version of *Phaser* (McCoy *et al.*, 2007), using the structure of *En. faecalis* DNA ligase

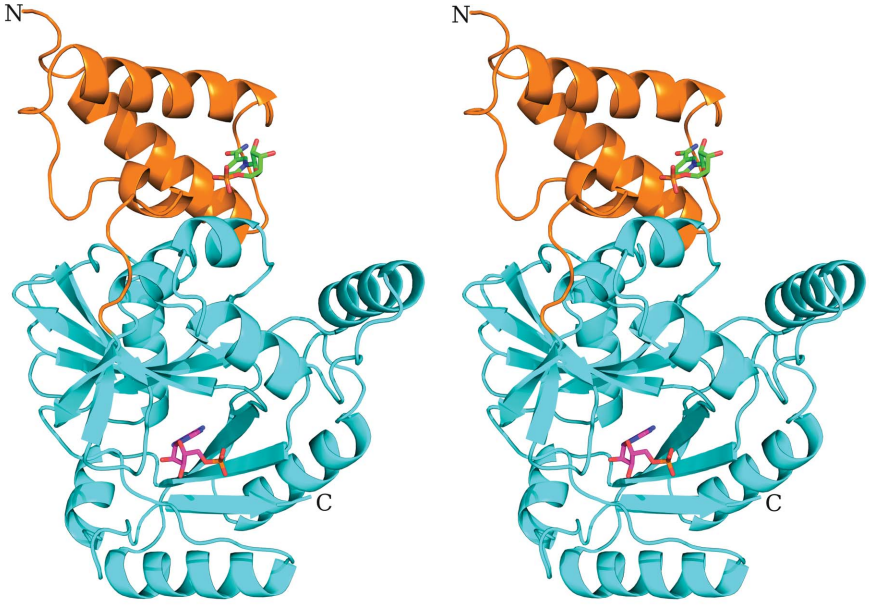

(*a*)

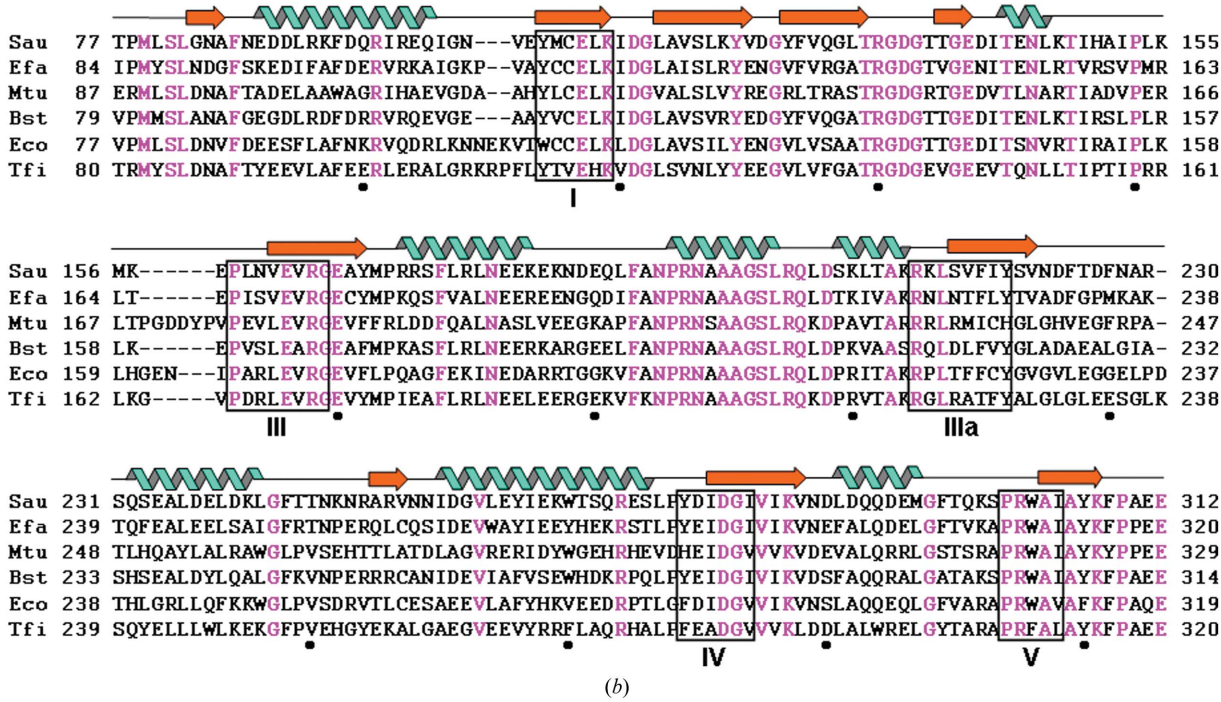

(*b*)

Figure 1
(*a*) Stereoview of the SauLigA structure. Subdomain 1a is shown in orange and subdomain 1b in cyan. NMN (green) and AMP (magenta) are positioned from the crystal structure of the EfaLigA–NAD complex (Gajiwala & Pinko, 2004). The labels N and C indicate the locations of the N- and C-termini. (*b*) A structure-based sequence alignment of SauLigA subdomain 1b (Sau) with those from *En. faecalis* (Efa), *M. tuberculosis* (Mtu), *B. stearothermophilus* (Bst), *E. coli* (Eco) and *T. filiformis* (Tfi). Secondary-structure elements of SauLigA are represented by 'noodles' (α-helices) and arrows (β-strands). They are colored blue for helices and orange for strands. Identical residues are highlighted in magenta. The conserved motifs are boxed in black. Every 20th residue is indicated by a black dot.

(Gajiwala & Pinko, 2004; PDB code 1ta8) as the search probe. After molecular replacement, maximum-likelihood-based refinement of the atomic positions and temperature factors was performed with *REFMAC* (Murshudov *et al.*, 1997) and the atomic model was built with the program *O* (Jones *et al.*, 1991). Water molecules were first placed automatically with *REFMAC*/*ARP* (Perrakis *et al.*, 1999) and were verified manually for consistency using difference electron-density maps and plausible hydrogen-bonding interactions. Eight sulfate molecules were modeled in the electron-density map and showed clear tetrahedral symmetry; they were likely to be a result of the addition of 2.1–2.5 *M* ammonium sulfate during crystallization. The stereochemical quality of the final models was assessed using *PROCHECK* (Laskowski *et al.*, 1993). Crystallographic statistics for the final models are shown in Table 1. Figures were prepared with *PyMOL* (DeLano, 2002).

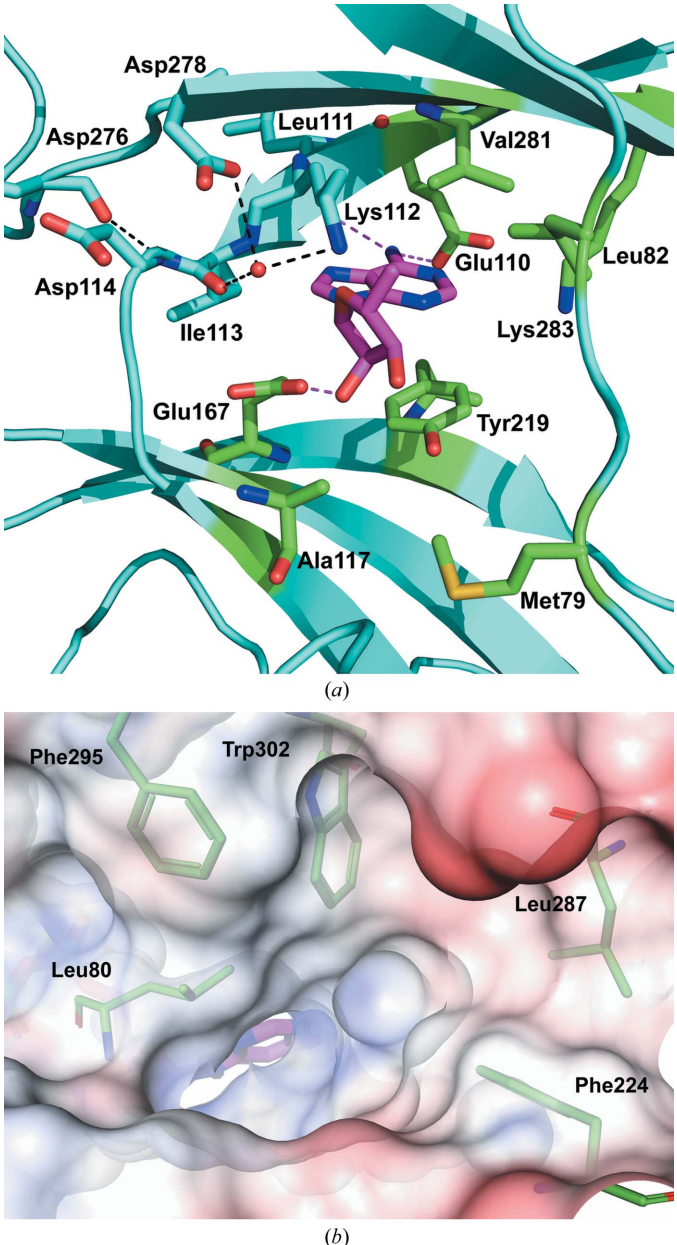

Figure 2
(*a*) SauLigA active site. The adenine ribose moiety (magenta) is positioned from the crystal structure of the EfaLigA–NAD complex. The critical side chains are shown in ball-and-stick representation and labeled, with hydrogen bonds shown as dashed lines. Residues involved in interactions with adenine are colored green. (*b*) A surface view of SauLigA with modeled adenosine (magenta) looking into the unique 'C2 tunnel'. The hydrophobic residues are shown as green ball-and-stick representations.

3. Results and discussion

3.1. Overall structure

The crystal structure of the adenylation domain of DNA ligase from *S. aureus* was determined at 1.8 Å (Apo1) and 1.9 Å (Apo2) resolution by molecular-replacement methods using the structure of *En. faecalis* DNA ligase (Gajiwala & Pinko, 2004; PDB code 1ta8) as the search probe. The two proteins share 57% sequence identity. A summary of data-collection and refinement statistics is reported in Table 1. The overall structure is very similar to those of other prokaryotic adenylation domains, displaying a two-subdomain architecture with approximate dimensions of 73 × 40 × 47 Å (Fig. 1). The smaller N-terminal domain 1a (residues 2–70) is mainly composed of two α-helices and is involved in NMN recognition. This subdomain contains a long loop that connects it to the larger C-terminal domain 1b (71–309) bearing an AMP-binding site in the crystal structure. Subdomain 1a is known to be flexible and adopts a different spatial disposition relative to subdomain 1b (Gajiwala & Pinko, 2004).

The structures of the two crystallographically independent SauLigA molecules in the triclinic crystals (Apo1) are almost identical, with r.m.s. differences of the main-chain atoms of about 0.2 Å. The apo structures in the triclinic (Apo1) and orthorhombic (Apo2) forms superimpose with an r.m.s. deviation of 1.5 Å. Significant conformational changes between the two crystal forms occur at surface residues 33–53 (r.m.s. deviation of 4.3 Å). These residues are involved in different crystal-packing interactions. The structure of the triclinic crystal is used for structural descriptions and comparisons unless otherwise stated.

3.2. NAD^+-binding site

Superposition of the individual subdomains of SauLigA onto the complex of *En. faecalis* DNA ligase (EfaLigA) with NAD provides a structural basis for modeling the SauLigA–NAD complex and reveals the key residues involved in NAD^+ recognition in SauLigA. NAD fits into the active-site pocket without significant steric conflicts. The preformed NAD^+-binding pocket and the ability to fit NAD into the EfaLigA active site without significant steric conflict suggest that the binding of NAD induces little conformational change in subdomain 1b (Fig. 2*a*).

The adenylation domain is composed of five conserved sequence motifs (I, III, IIIa, IV and V) in NAD^+-dependent ligases (Shuman & Schwer, 1995; Shuman & Lima, 2004). Lys112 in motif I, which is located between two antiparallel β-sheets of subdomain Ib (Fig. 2*a*), is a critical nucleophile for the adenylation reaction and as such is strictly conserved across many families of covalent nucleotidyl transferases. Lys112 is well defined by the electron density and its side chain is oriented to form water-mediated hydrogen bonds with the side chain of Asp278 and the main chain of Ile113. Mutagenesis of Lys112 to Arg or Gln in both the *E. coli* and *T. thermophilus* DNA ligases causes a significant reduction in the formation of the ligase-adenylate intermediate and abolishes nick-joining activity (Luo & Barany, 1996; Sriskanda *et al.*, 1999; Zhu & Shuman, 2005).

Asp114 in motif I forms a hydrogen bond to the carbonyl backbone of Asp277 and its side chain is solvent-exposed, forming hydrogen bonds to several water molecules. Mutation of the equivalent of Asp114 in the *E. coli* and *T. thermophilus* DNA ligases showed the

essential role of this conserved Asp during the deadenylation step (Luo & Barany, 1996; Zhu & Shuman, 2005).

Based upon superposition of SauLigA with the EfaLigA–NAD complex, the interactions with the AMP moiety are conserved. The adenine ring is stacked against the side chain of Tyr219 in a deep pocket composed of Leu82, Ala117, Val281, Met79 and the aliphatic portions of Glu167, Tyr219 and Lys283. Interestingly, MtuLigA has a histidine residue in at the structurally equivalent position of Tyr219 that forms a stacking interaction with the adenine moiety (Srivastava, Tripathi *et al.*, 2005). The 6-amino group of the adenine ring forms hydrogen-bond interactions with the carbonyl backbone of Leu111 and the Glu110 side chain. The Glu167 side chain in motif III is involved in a hydrogen-bond interaction with the 2′-OH group of the ribose ring. The mutation of Glu167 to Asp or Gln abolishes LigA nick-joining activity (Zhu & Shuman, 2005). This interaction involving the corresponding Glu residue is not observed in TfiLigA owing to differences in the AMP conformations (Lee *et al.*, 2000).

Unlike the EfaLigA–NAD complex structure, which showed tightly bound NMN in subdomain Ia even after the deadenylation step, subdomain Ia in SauLigA does not show NMN binding in spite of the similar preparation of the protein. In SauLigA, the nicotinamide moiety can interact with two conserved residues Tyr18 and Tyr22 as observed in the EfaLigA–NAD complex. Mutation of structurally equivalent residues in EcoLigA abolishes or reduces the sealing of a 5′-phosphate nick and adenylyl transfer from NAD^+ (Sriskanda & Shuman, 2002).

3.3. Insight into stucture-based inhibitor design of NAD^+-dependent DNA ligases

A diverse range of inhibitors of NAD^+-dependent DNA ligase have been identified (Dwivedi *et al.*, 2008). Two classes of inhibitors, pyridochromanones and glycosyl derivatives, inhibit NAD^+-dependent DNA ligases by competing with NAD^+ binding and do not interact with DNA. The pyridochromanones exhibit bactericidal activity against *S. aureus* in the low $\mu g\ ml^{-1}$ range without affecting eukaryotic cells up to $60\ \mu g\ ml^{-1}$ (Brötz-Oesterhelt *et al.*, 2003; Srivastava, Dube *et al.*, 2005). The third class, quinoline analogues, are not a competitive NAD^+ inhibitor and apparently act by binding to the other sites in the enzyme (Ciarrocchi *et al.*, 1999). Although these molecules show moderate and specific inhibition of DNA ligases, there are no known examples of marketed antibiotics owing to their poor drug-like properties.

The cofactor-binding sites of bacterial DNA ligases have been targeted for the identification of competitive inhibitors as distinct structural differences have been observed compared with eukaryotic DNA ligases. Like other bacterial adenylation-domain structures, the SauLigA adenylation-domain structure reveals a distinct tunnel which is in part composed of the loop region (Thr77–Leu82), perpendicular to the NAD^+-binding pocket and exposing the C2 atom of the adenine moiety. This tunnel does not exist in human DNA ligase I and other ATP-dependent DNA ligases and has been identified as a potential selecitivity pocket (Nandakumar *et al.*, 2007).

This unique tunnel ('C2 tunnel') is lined with hydrophobic residues including Leu80, Phe224, Leu287, Phe295 and Trp302. It is noteworthy that none of these hydrophobic residues is strongly conserved. Importantly, the Leu80 side chain at the mouth of the tunnel points inside the tunnel and forms a narrow funnel in the SauLigA structure. It will require significant conformational changes in the Leu80 side chain to accommodate alkyl derivatives at the C2 position of the adenine moiety. In contrast, the corresponding side chains of residues in *En. faecalis* (Tyr87), *M. tuberculosis* (Leu90), *B. stearothermophilus* (Met82), *E. coli* (Leu80) and *T. filiformis* (Tyr83) point toward solvent-exposed surface and the corresponding tunnels are wide enough to accommodate alkyl derivatives at the C2 position of the adenine moiety. With regard to the design of a potential broad-spectrum inhibitor, the sequence variations in the C2 tunnel need be considered.

In conclusion, the crystal structure of *S. aureus* LigA reveals a preformed active-site NAD^+-binding site with potential key residues for NAD^+ recognition similar to those of other NAD^+-dependent DNA ligases. In addition to the active site, the adenylation domain of DNA ligase from *S. aureus* contains the narrow 'C2 tunnel' for potential use in inhibitor design. The SauLigA structure thus provides a basis for a more integrated understanding of substrate recognition and catalysis and will also be of help in the development of small-molecule inhibitors.

References

Brötz-Oesterhelt, H., Knezevic, I., Bartel, S., Lampe, T., Warnecke-Eberz, U., Ziegelbauer, K., Häbich, D. & Labischinski, H. (2003). *Biol. Chem.* **278**, 39435–39442.

Ciarrocchi, G., MacPhee, D. G., Deady, L. W. & Tilley, L. (1999). *Antimicrob. Agents Chemother.* **43**, 2766–2772.

DeLano, W. L. (2002). *The PyMOL Molecular Graphics System.* DeLano Scientific, San Carlos, California, USA. http://www.pymol.org.

Dwivedi, N., Dube, D., Pandey, J., Singh, B., Kukshal, V., Ramachandran, R. & Tripathi, R. P. (2008). *Med. Res. Rev.* **28**, 545–568.

Furuya, E. Y. & Lowy, F. D. (2006). *Nature Rev. Microbiol.* **4**, 36–45.

Gajiwala, K. & Pinko, C. (2004). *Structure*, **12**, 1449–1459.

Jones, T. A., Zou, J.-Y., Cowan, S. W. & Kjeldgaard, M. (1991). *Acta Cryst.* A**47**, 110–119.

Kaczmarek, F. S., Zaniewski, R. P., Gootz, T. D., Danley, D. E., Mansour, M. N., Griffor, M., Kamath, A. V., Cronan, M., Mueller, J., Sun, D., Martin, P. K., Benton, B., McDowell, L., Biek, D. & Schmid, M. B. (2001). *J. Bacteriol.* **183**, 3016–3024.

Kornberg, A. & Baker, T. A. (1992). *DNA Replication*, edited by A. Kornberg & T. A. Baker, pp. 307–322. New York: W. H. Freeman & Co.

Laskowski, R. A., MacArthur, M. W., Moss, D. S. & Thornton, J. M. (1993). *J. Appl. Cryst.* **26**, 283–291.

Lee, J. Y., Chang, C., Song, H. K., Moon, J., Yang, J. K., Kim, H.-K., Kwon, S.-T. & Suh, S. W. (2000). *EMBO J.* **19**, 1119–1129.

Lindahl, T. & Barnes, D. E. (1992). *Annu. Rev. Biochem.* **61**, 251–281.

Lowy, F. D. (1998). *N. Engl. J. Med.* **339**, 520–532.

Luo, J. & Barany, F. (1996). *Nucleic Acids Res.* **24**, 3079–3085.

McCoy, A. J., Grosse-Kunstleve, R. W., Adams, P. D., Winn, M. D., Storoni, L. C. & Read, R. J. (2007). *J. Appl. Cryst.* **40**, 658–674.

Murshudov, G. N., Vagin, A. A. & Dodson, E. J. (1997). *Acta Cryst.* D**53**, 240–255.

Nandakumar, J., Nair, P. A. & Shuman, S. (2007). *Mol. Cell*, **26**, 257–271.

Otwinowski, Z. & Minor, W. (1997). *Methods Enzymol.* **276**, 307–326.

Perrakis, A., Morris, R. & Lamzin, V. S. (1999). *Nature Struct. Biol.* **6**, 458–463.

Shuman, S. & Lima, C. D. (2004). *Curr. Opin. Struct. Biol.* **14**, 757–764.

Shuman, S. & Schwer, B. (1995). *Mol. Microbiol.* **17**, 405–410.

Singleton, M. R., Håkansson, K., Timson, D. J. & Wigley, D. B. (1999). *Structure*, **7**, 35–42.

Sriskanda, V., Schwer, B., Ho, C. K. & Shuman, S. (1999). *Nucleic Acids Res.* **27**, 3953–3963.

Sriskanda, V. & Shuman, S. (2002). *J. Biol. Chem.* **277**, 9695–9700.

Srivastava, S. K., Dube, D., Tewari, N., Dwivedi, N., Tripathi, R. P. & Ramachandran, R. (2005). *Nucleic Acids Res.* **33**, 7090–7101.

Srivastava, S. K., Tripathi, B. P. & Ramachandran, R. (2005). *J. Biol. Chem.* **280**, 30273–30281.

Timson, D. J., Singleton, M. R. & Wigley, D. B. (2000). *Mutat. Res.* **460**, 301–318.

Tomkinson, A. E., Vijayakumar, S., Pascal, J. M. & Ellenberger, T. (2006). *Chem. Rev.* **106**, 687–699.

Wilkinson, A., Day, J. & Bowater, R. (2001). *Mol. Microbiol.* **40**, 1241–1248.

Zhu, H. & Shuman, S. (2005). *J. Biol. Chem.* **280**, 12137–12144.